Reprinted from Analytical Chemistry, 1991, 63.

Characterization of Polycyclic Aromatic Compounds on Surfaces Using Ion-Beam-Induced Desorption and Multiphoton Resonance Ionization

D. M. Hrubowchak, M. H. Ervin, and Nicholas Winograd*

Department of Chemistry, The Pennsylvania State University, 152 Davey Laboratory, University Park, Pennsylvania 16802

Multiphoton resonance ionization (MPRI) has been combined with ion-beam-induced desorption to examine polycyclic aromatic compounds (PAC's) present on surfaces. The results show that it is possible to obtain extremely high-quality mass spectra of these compounds with subfemtomole sensitivity limits. Although the degree of ionization selectivity of atomic species is much lower than for MPRI of molecules, we show that it is possible to control the degree of photofragmentation by varying the laser intensity. Spectra obtained by MPRI, by nonresonant multiphoton ionization (MPI), and directly by secondary ion mass spectrometry (SIMS) are quantitatively compared. For pyrene, the molecular ion signal is more than 10 times larger for MPRI than for MPI and more than 100 times larger than with SIMS. From the measured intensities, we estimate the fraction of pyrene molecular ions formed in the SIMS mode is on the order of 10^{-4}. Finally, we demonstrate that mixtures of PAC's are readily detected by examining a cocktail of codeposited benzo[*a*]pyrene, dibenz[*ac*]-anthracene, triphenylene, and pyrene. In general, we propose that this approach is a powerful new method for detecting low concentrations of complex molecules adsorbed on surfaces.

INTRODUCTION

Mass spectrometric characterization of thermally labile molecules is now a well-established methodology. The key to the emergence of this important field is the discovery that a variety of molecules can be desorbed directly from the solid state by use of either energetic particles (*1*, *2*) or pulsed laser beams (*3*, *4*). The molecules can be ionized by collisions during the desorption event or subsequently by electron impact, chemical ionization, or laser excitation. The separation of the desorption event from the ionization event is important to improve the sensitivity since most of the desorbed flux consists of neutral particles (*5*). Moreover, matrix ionization effects are not nearly as severe when postionization techniques are used (*6*).

Our efforts have been focused on utilizing multiphoton resonance ionization (MPRI) spectroscopy to ionize particles desorbed from surfaces with kiloelectronvolt ion beams (*7*). This approach offers several unique advantages when compared to other related methods. First, ion-beam desorption, as opposed to laser or thermal desorption, is extremely efficient at selectively removing molecules from only the top layer of a solid (*8*). This characteristic means that the signals are specific to the surface concentration of the analyte. As an

0003-2700/91/0363-0225$02.50/0

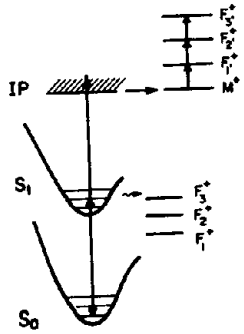

Figure 1. Schematic diagram illustrating the MPRI process used for detecting ion-beam-desorbed neutral molecules.

additional bonus, the theory of ion/solid interactions is highly developed (*9*). This important fundamental aspect allows valuable mechanistic insight into the nature of the desorption event. Second, MPRI detection offers selective ionization by use of relatively low-power pulsed lasers (*10*). The low-power requirement allows the use of a large ionization volume. This aspect of the technique results in more efficient sampling than with ionization schemes based on electron impact or focused lasers. Third, the pulsed nature of the radiation adds another dimension of selectivity provided by the built-in availability of a time-of-flight (TOF) mass spectrometer detector. These detectors exhibit inherently very high transmission efficiency (*11*). Finally, MPRI can be an extremely efficient means of producing ions. For the case of atomic species, we have already demonstrated ionization efficiencies of several percent, yielding detection limits of just a few hundred atoms spread over a 1-cm^2 surface (*10*).

Special problems arise when attempting to utilize this technology for the detection of molecules on surfaces using ion beam induced desorption. Computer simulations (*12*) as well as a limited number of experimental studies (*13, 14*) suggest that the molecules desorb in a variety of highly excited vibrational and rotational states, with the largest population remaining in the ground-state electronic manifold. Two approaches have been successfully pursued in connection with other desorption schemes that will likely have relevance to the ion-beam-induced desorption technique. In one scheme, the molecules are first entrained and cooled by a supersonic jet of a noble gas (*15*). The advantage of this step is that the target molecules are cooled into a single spectroscopic state. The MPRI process can then be highly selective and efficient. A disadvantage is that only a very small fraction of the molecules can be trapped into the jet, dramatically reducing the sensitivity. In a second approach, the molecules are ionized directly by a laser tuned to a wavelength associated with an electronic transition of the molecule. Since there are a high density of occupied vibrational and rotational states in the ground-state manifold and since each of these states can connect with a real level in the excited-state manifold, a degree of selectivity is lost. This simplified scheme, however, offers major advantages in sensitivity due to the increased sampling efficiency. A schematic energy level diagram of this process is shown in Figure 1. There have already been elegant experimental demonstrations of attomole detection limits when this mode of operation is coupled to laser desorption (*16*).

In this paper, we demonstrate that MPRI can be an effective means of postionizing molecules desorbed from surfaces by particle beams. We have chosen a set of polycyclic aromatic compounds (PAC's) as models for evaluating the characteristics of this approach. The compounds are, of course, environmental health hazards because of their acute carcinogenic and mutagenic behavior. Moreover, there are many applications where surface detection of PAC's is desirable without

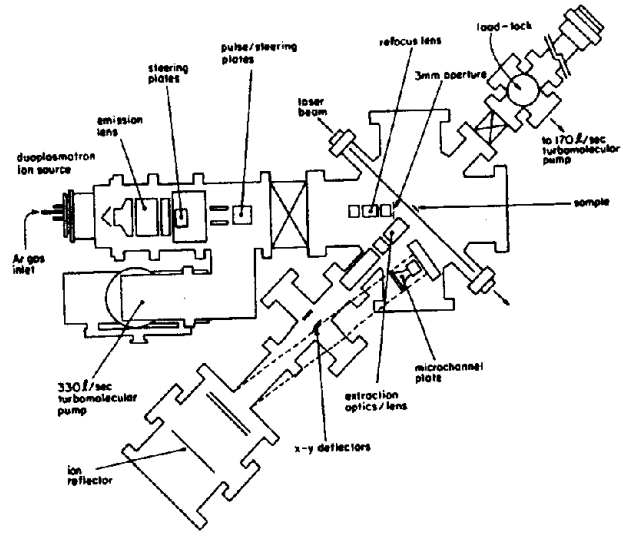

Figure 2. Schematic diagram of the MPRI apparatus.

resorting to elaborate sample pretreatment. Our results show that, indeed, it is possible to characterize small fractions of a monolayer of PAC's on both conducting and insulating surfaces with subfemtomole detection limits. We also compare the results of MPRI postionization to secondary ion mass spectra (SIMS) and to nonresonant ionization spectra where important structural information can be obtained through controlled photofragmentation. These comparisons allow estimation of the fraction of desorbed particles which are neutral and which are ionized. Finally, we discuss the prospects for this methodology and additional experimental procedures for further reducing the detection limits.

EXPERIMENTAL SECTION

The basic experimental apparatus has been described elsewhere (*10, 17*). Briefly, the vacuum chamber consists of an ion-pumped Perkin-Elmer Ultek TNB-X chamber with a base pressure of 5 × 10^{-9} Torr. The system is equipped with a load-lock assembly pumped by a Balzers TSU170 170 L/s turbomolecular pump. This assembly allows new samples to be inserted in less than 10 min. A schematic diagram illustrating the arrangement of the important components is shown in Figure 2.

During the experiment, a 5.6-μs pulse of primary Ar^+ ions (34 μA, 10 keV) is generated by a Physicon Model DP10-01 duoplasmatron source. The primary ion beam has a spot diameter of 1 mm and is incident on the target at an angle of 45°. The laser system consists of a Quanta-Ray Model PDL-2 dye laser pumped by a Quanta-Ray Model DCR-2A Nd:YAG laser triggered at a 30-Hz repetition rate. Frequency doubling of the dye laser output is accomplished by using a Quanta-Ray Model WEX-1 wavelength extension unit. Laser energy is monitored with a Scientech Model 362 power meter.

For all experiments reported here, ionization is initiated with 280-nm (4.407-eV) radiation. This wavelength is sufficient to excite most aromatic molecules to the first excited state ($S_1 \leftarrow S_0$). When two photons are absorbed, the energy sum exceeds the ionization potential of a large number of PAC's as shown in Table I. The 280-nm radiation is produced from Exciton Rhodamine 590 dye in CH_3OH, yielding 5 mJ/6 ns pulse (8.3 × 10^5 W) after frequency doubling. Depending on the alignment, the cross-sectional area of the unfocused laser beam ranges from 0.33 to 0.66 cm^2, yielding power densities of (1.26–2.5) × 10^6 W/cm^2. For experiments requiring higher power densities, the 280-nm beam could be tightly focused above the sample by using a 30-cm lens to a calculated cross-sectional area of 3.2 × 10^{-3} cm^2 or a power density of 2.6 × 10^8 W/cm^2.

Following resonant postionization, the photoions are extracted into a reflecting time-of-flight (TOF) mass spectrometer and are detected by a Galileo Electro-Optics Corp. Model FTD 2002 dual microchannel plate (MCP) assembly. The output pulses from the MCP are processed in one of three ways depending upon the particular study. For analog signals, a Stanford Research Systems

Table I

molecule	structure	solvent	substrate	IP_r[a] eV
(I) carbazole	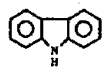	acetone	Au	7.25[18]
(II) pyrene	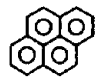	benzene	Au	7.42[19]
(III) benzo[*a*]pyrene	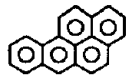	benzene	Si	7.12[19]
(IV) dibenz[*ac*]anthracene	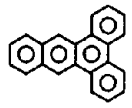	benzene	Si	7.39[20]
(V) triphenylene	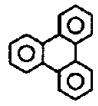	benzene	Si	7.88[20]
(VI) coronene	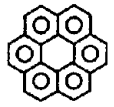	benzene	Si	7.29[20]

[a] IP = ionization potential.

Model SR 250 gated integrator is used as a boxcar averager. Time-of-flight mass spectra are recorded by routing the analog signal from the MCP to a 100-MHz Digital Signal Processing (DSP) Technology Model 2001AS transient recorder with a DSP Model 4100 averaging memory and averaging over 1024 laser pulses (34 s). For single-ion-counting experiments, the output signal is processed digitally by using a Princeton Applied Research (PAR) Model 1121A amplifier/discriminator unit and a gated PAR Model 1112 photon counter processor.

Analog signals are digitized with 8-bit precision by use of the transient recorder and are transferred to a Digital Equipment Corp. MicroVaxII by a CAMAC interface. A full-scale analog signal corresponds to 512 mV. The peak intensities for all reported spectra are obtained by use of the same gain conditions for the MCP and are therefore directly comparable. It is possible to roughly estimate the number of ions/second associated with the millivolt intensity scale. A typical mass peak has a full-width at half-maximum of about 250 ns. When terminated into 50 Ω, a 1-mV signal would correspond to 2.6 ions/laser shot or 78 ions/s, assuming an MCP gain of 1.2×10^7.

We have not converted the time scale reported in the TOF spectra to a mass scale since there are a number of variables associated with these values. For example, the starting time of the experiment is associated with initiation of the ion pulse and actuation of the transient digitizer 1.0 μs later. These events follow the charging of the flashlamps by several hundred microseconds. The ion pulse requires about 3 μs to reach the target and is 5.6 μs in duration. The Q-switch is opened about 100 ns after the falling edge of incident ion pulse arrives at the target. All of these processes contribute a fixed 7.70-μs timing offset to the TOF spectra. Moreover, the flight times of the SIMS ions and the ions created by the laser beam are quite different since they experience different extraction fields. Thus, we have always assigned unknown mass peaks by calculating their positions relative to known mass peaks. More details of the pulsing/timing sequence have been previously reported (*10*).

A background spectrum obtained by blocking the MPRI laser is subtracted from each TOF spectrum. The main source of background is secondary ions that arrive at the detector during an analysis. The intensity of these ions is generally less than 1% of the base peak signal amplitude in the TOF spectra and are typically found only at low masses. In general, the PAC's studied in this work have significant vapor pressures at room temperature. As expected, a gas-phase signal is observed in the absence of any ion bombardment due to vacuum sublimation of the molecular film. Consequently, a gas-phase spectrum, obtained by turning off the incident ion pulse while leaving the MPRI laser on, is subtracted from each waveform. In general, the gas-phase component comprises ~10% of the total ion desorbed signal amplitude for the PAC's investigated.

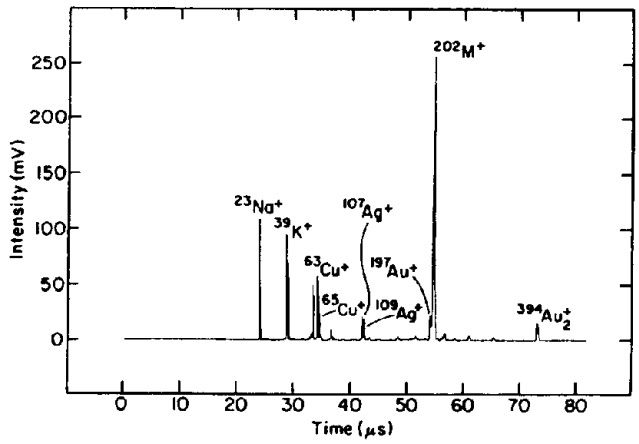

Figure 3. Time-of-flight mass spectrum of a thick film of pyrene molecules desorbed from the surface of a gold substrate. MPRI was accomplished with 280-nm laser radiation operated at a power density of 1.4×10^6 W/cm^2.

Secondary ion mass spectra could be obtained by adjustment of the reflector potentials to allow efficient transmission of the positive SIMS ions to the MCP. To perform these measurements, the incident ion pulse is narrowed from the value of 5.6 μs employed for neutral detection to several hundred nanoseconds so as to resolve the individual charged components. The output SIMS signal from the MCP is processed in the same fashion as the laser experiments described above.

The PAC's investigated in this work are listed in Table I. Prior to sample deposition, each substrate was ultrasonically cleaned in ethanol and mounted on a copper backplate. For experiments on bulk samples where sensitivity is not an issue, milligram quantities of the molecule of interest were dissolved in the appropriate solvent and placed on a clean silicon wafer or a polycrystalline gold foil. The solvent was allowed to evaporate in air before insertion into the chamber via the load-lock assembly. After several seconds, crystallites of the chosen PAC are observed, probably corresponding to the formation of several hundred monolayers of material. For trace analysis experiments, pyrene was dissolved in ~10 mL of HPLC-grade benzene and diluted to volume with spectrophotometric-grade methanol to prepare a 10^{-3} M stock solution. A 10^{-5} M pyrene/stock solution was prepared by analytical dilution. A 1-μL aliquot was deposited onto the surface of a polycrystalline gold foil. The amount of pyrene in the analysis zone is then estimated to be 4.5×10^{-12} mol. Following air evaporation of the solvent, the sample is inserted into the chamber via the load-lock assembly for analysis. This procedure is repeated several times to provide independent analyses. The PAC's studied were obtained from the Aldrich Chemical Company and were used without further purification.

RESULTS AND DISCUSSION

The TOF mass spectrum obtained by MPRI detection of neutral pyrene molecules desorbed from the surface of a gold substrate is shown in Figure 3. In this case, the laser was tuned to 280 nm and operated at a power density of 1.4×10^6 W/cm^2 for an unfocused 8.8-mm-diameter laser beam. The peaks below 50 μs represent nonresonant ionization of substrate impurities such as Na, K, Cu, and Ag. Weak intensities for Au and Au_2 are visible, also due to nonresonant photon absorption. The pyrene molecular ion signal is very obvious, with little or no fragmentation seen in the spectrum.

Upon focusing the beam to 0.635 mm (1.7×10^8 W/cm^2) to induce nonresonant multiphoton ionization (MPI) (*21*), extensive photofragmentation is observed as demonstrated in Figure 4. The molecular ion signal drops by a factor of ~20, commensurate with an increase in intensity of various low-mass hydrocarbon fragments. Moreover, there is a sub-

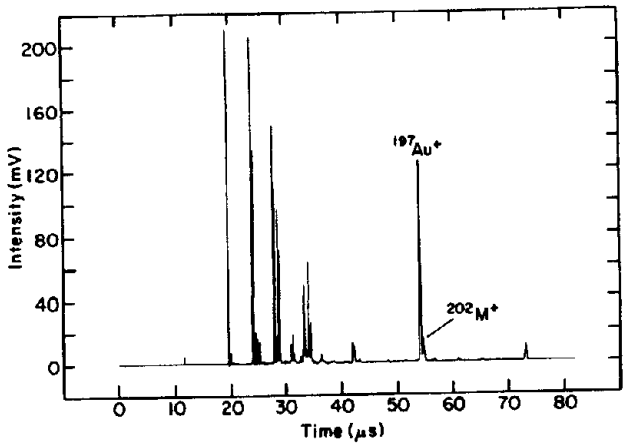

Figure 4. Time-of-flight MPI spectrum of neutral pyrene molecules obtained by focusing a 280-nm laser beam. The power density was 1.7×10^8 W/cm^2.

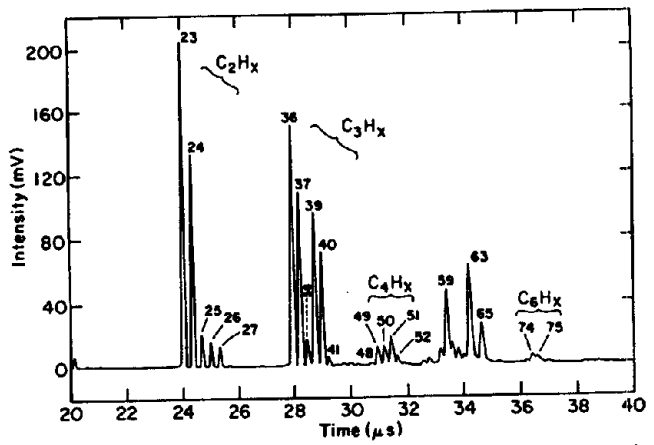

Figure 5. Portion of the TOF MPI spectrum presented in Figure 4 showing the 20–40 μs time segment. Peaks arising from photoinduced fragmentation of pyrene are observed corresponding to C_2H_x, C_3H_x, C_4H_x, and C_6H_x species. The mass assignments are labeled in the figure.

stantial growth in intensity of the elemental Au substrate peak as the efficiency of nonresonant ionization is increased upon focusing. Expansion of the time window between 20 and 40 μs shown in Figure 4 allows identification of the low-mass ions, as seen in Figure 5. The photofragments of pyrene consist primarily of C_2H_x, C_3H_x, C_4H_x, and C_6H_x species. The most plausible explanation for the photofragmentation of the pyrene molecular ion (M^+) involves multiple photon absorption at high-laser-power densities of M^+ into fragmenting states (F_r) as illustrated in Figure 1. These fragmentation spectra are very similar to those reported for the MPI of pyrene after laser desorption into a supersonic jet (*22*).

The SIMS spectrum of pyrene obtained by using the same reflectron analyzer as used for the laser ionization experiments is shown in Figure 6. The pyrene molecular ion signal is about 10 times lower than the signal obtained with MPI and about 130 times lower than the MPRI spectrum. The ubiquitous $^{23}Na^+$ and $^{39}K^+$ peaks are also observed as well as a $^{63}Cu^+$ signal originating from the mounting backplate. We have measured the ion fraction for pyrene desorbed from a Au substrate by boxcar averaging the postionized neutral and ionic analog molecular ion signals. Several corrections to the data have been applied in order to directly compare the ion and neutral yields. First, a gas-phase component resulting from vacuum sublimation of pyrene was subtracted from the molecular ion amplitude, yielding an intensity solely due to ion-initiated desorption. The gas-phase signal was 8% of the pyrene M^+ intensity. Second, the SIMS data were obtained by use of a much smaller incident ion current since a much narrower

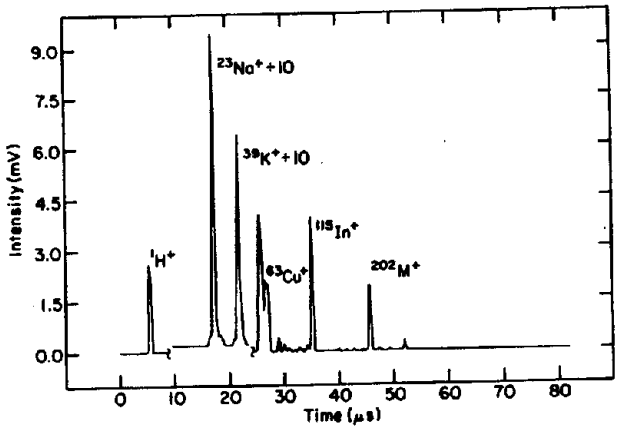

Figure 6. Time-of-flight positive SIMS spectrum of pyrene desorbed from the surface of a gold substrate by using a 510-ns incident Ar^+ ion pulse.

pulse width is required to achieve acceptable mass resolution. The intensities are therefore corrected for the relative incident ion fluences. Third, the MPRI signal was adjusted to account for the fraction of molecules that are in the laser beam. This is a critical parameter for any experiment using a laser as an ionization source. The spatial overlap between the desorbed molecules and the laser can be increased by enlarging the beam diameter. Although the overall sensitivity for a measurement is increased, resolution is sacrificed since the neutral particles are photoionized in different regions of the beam profile. This leads to time broadening, resulting from inequivalent extraction energies. Consequently, there is a trade-off between mass resolution and laser beam width that must be considered when using MPRI. In our experiment, a 5.6-μs ion pulse width is employed, implying that 25% of the desorbed molecules are spatially overlapped with the photon field (*17*). Finally, we assume that the transmission efficiencies of the neutral and ionic particles are equivalent. Following data normalization, we measured a pyrene ion fraction of $\sim 1.7 \times 10^{-2}$. This value does not include a correction for the ionization efficiency of pyrene by MPRI and therefore serves as an upper limit to the ion fraction. Assuming typical MPRI efficiencies of 0.1–1%, the ion fraction could be as low as 10^{-4}–10^{-5}. Thus, from the above results it is clear that the vast majority of the desorbed molecules eject from the surface as neutrals. This fact is a major driving force for applying MPRI to trace analytical problems where efficient sampling is important for increasing sensitivity.

The intensity of the molecular ion signal is clearly a strong function of the laser power. It is possible to qualitatively examine the mechanism of photoionization from this dependence. If two-photon ionization occurs through a resonant excitation and both transitions are saturated, then the ionization signal should be independent of the laser power. It either of the excitations are not saturated, the signal intensity should increase linearly with laser power. For nonresonant ionization, a squared dependence is usually expected. This condition is also expected for MPRI when neither excitation is saturated. In practice, observation of this behavior does not provide unequivocal evidence of the ionization mechanism. Photodissociation, which is also power dependent, may alter the predicted response. Moreover, it is difficult to maintain a constant ionization volume as the laser power is increased, especially for tightly focused beams.

The power dependence of the pyrene molecular ion intensity at 280 nm is shown in Figure 7 for an unfocused laser beam. The intensity increases with a slope of 1.2 at low power densities but reaches a plateau at a value of 7×10^5 W/cm^2. There is also a non-zero x-axis intercept associated with the lowest laser powers. Although we have not probed this region

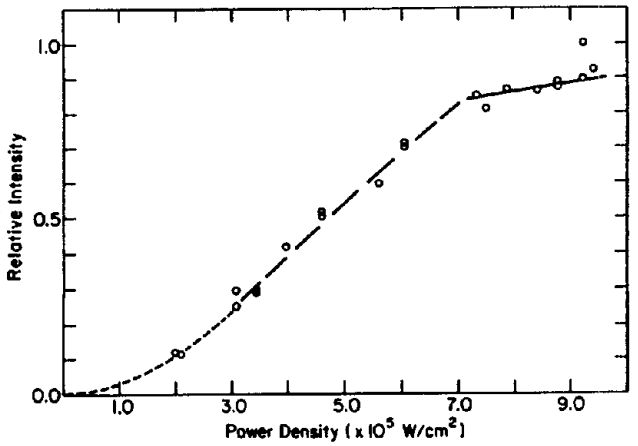

Figure 7. Response of the pyrene molecular ion intensity to laser power density for an unfocused 280-nm beam. The dashed and solid curves display the transition of the ionization signal from a two-photon dependence (- - -) to a one-photon dependence (– –) followed by saturation (—).

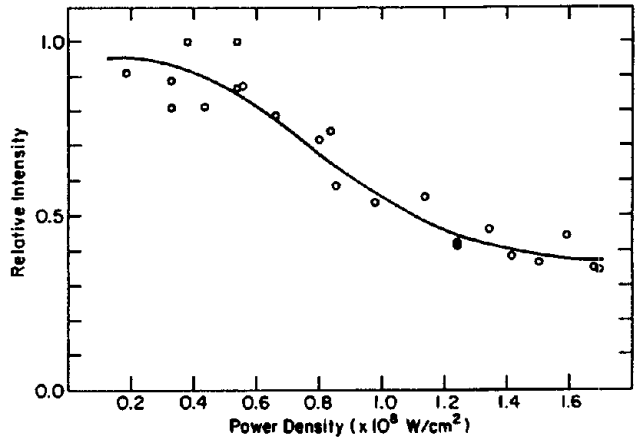

Figure 8. Effect of laser intensity on the pyrene molecular ion signal for a focused 280-nm beam. The absolute signal intensities are ~ 20-fold lower than those presented in Figure 7 due to a decreased ionization volume. The solid curve (—) does not represent any functional form and is presented only as a guide to the eye.

in detail, the behavior suggests that the signal is increasing with a squared dependence. The data in Figure 7 are consistent with the notion that, at the lowest power densities, the ionization proceeds through two unsaturated resonant excitations. In the linear region, presumably the resonant excitation becomes saturated, while both steps are saturated in the plateau region. We note that these data are not complicated by photoinduced fragmentation of pyrene. At all laser powers in this range, no significant differences in the low-mass part of the spectrum could be discerned.

Very different behavior is observed when the laser beam is focused as seen in Figure 8. In this case, the molecular ion signal is seen to decrease with laser power at $\sim 5 \times 10^7$ W/cm^2. This decline is almost certainly associated with photoinduced fragmentation. This fragmentation is clearly seen in the low-mass region of Figures 4 and 5. We chose to employ a relative intensity scale in Figures 7 and 8 for display purposes. In particular, the absolute intensities presented in Figure 8 are ~20-fold lower than those depicted in Figure 7. Presumably, this decrease is associated with a decrease in ionization volume upon focusing.

The MPRI spectra of pyrene desorbed from an ion-bombarded surface are of very high quality, suggesting that this technique may be an important new approach for the trace analysis of surfaces. We can make some preliminary estimates of the expected detection limits using existing data. Specifically, 1×10^{-11} mol of pyrene was deposited onto a 0.16-cm^2 gold surface. During the analysis cycle, the incident ions were focused into a 0.07-cm^2 beam spot. Consequently, only ~40% of the total available analyte surface area was probed by the ion beam during the experiment. The concentration of pyrene in the ion-beam sampling area is therefore 4×10^{-12} mol. This target yielded 2.1×10^3 counts/μA of incident current during a 5-min analysis time (9000 laser shots). The background signal is approximately 1 count/μA during this same time interval. At an incident current of 100 μA and a signal/noise (S/N) ratio of 2, the detection limit is 6×10^{-16} mol present in the area probed by the ion beam. This limit corresponds to the detection of 4×10^8 molecules or 6×10^{-5} monolayers of analyte on the assumption that a 1 monolayer coverage contains 1×10^{14} molecules spread over 1 cm^2. Similar results were obtained on two other replicate samples with a relative standard deviation of 29%. A gas-phase signal originating from vacuum sublimation of the pyrene molecules is observed for each sample. This component comprised ~7% of the overall count rate for the independent analyses. Therefore, a large uncertainty exists in the initially deposited concentration of pyrene.

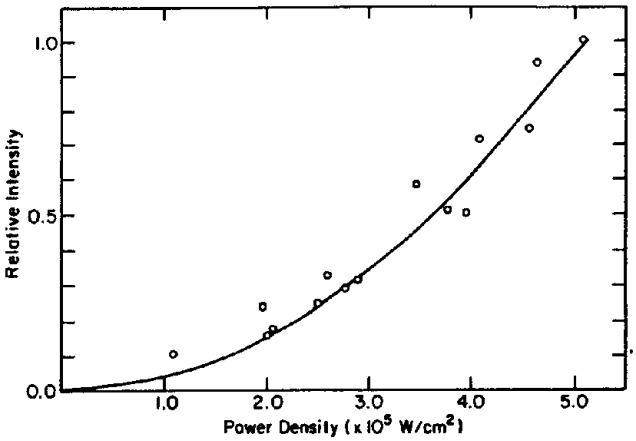

Figure 9. Intensity response of the carbazole molecular ion as a function of power density for an unfocused 287-nm laser beam. The solid curve (—) represents a $y = x^2$ function.

At this stage, we consider this detection limit to be an upper bound on the capability of the technique. As noted earlier, a detection limit of 200 atoms has been reported for In on Si. Assuming that the ionization efficiency of pyrene can be as high as 1% under the proper laser conditions, comparison to our previous work suggests that detection limits of just 20 000 molecules ($\sim 10^{-20}$ mol) are feasible.

We have examined the response of a variety of PAC's to ion bombardment and subsequent laser postionization. Carbazole has yielded one of the strongest signals we have observed to date. In this case, only a single molecular ion peak is found at an ionizing wavelength of 287 nm, corresponding to the carbazole molecular ion (*23*). The power dependence of this signal, however, exhibits different behavior than that found for pyrene. As seen in Figure 9, the molecular ion intensity increases as the square of the laser power. As noted above, this behavior is consistent with ionization that is occurring either through two unsaturated resonant excitations or by direct two-photon nonresonant excitation. The absence of fragmentation and the large intensity of the signal is indicative of a resonant process. We tested this hypothesis by focusing the laser beam to increase the power density further. Although the signal intensity decreases by ~20-fold, the power dependence transforms from a squared dependence to a linear dependence as seen in Figure 10. Again, the decrease in intensity presumably arises from the decreased ionization volume. The linear power dependence suggests that one of

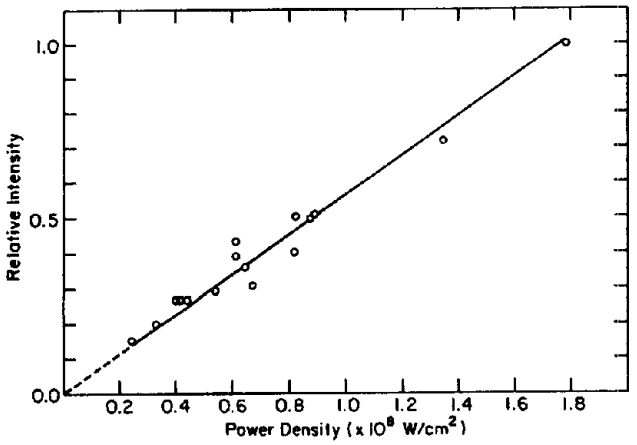

Figure 10. Intensity response of the carbazole molecular ion as a function of power density for a focused 287-nm laser beam. The absolute signal intensities are ~20-fold lower than those presented in Figure 9 due to a decreased ionization volume.

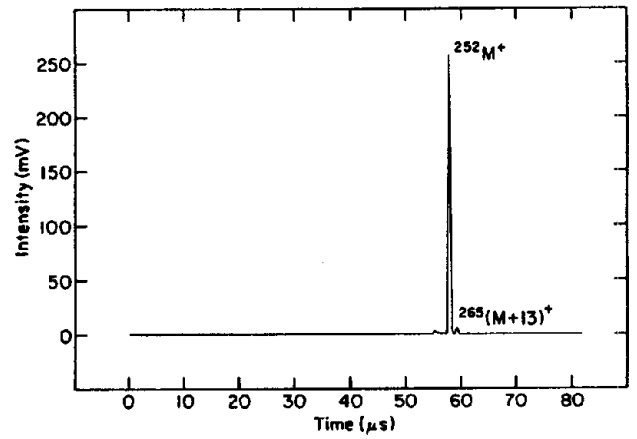

Figure 11. Time-of-flight mass spectrum of a thick film of benzo[*a*]pyrene molecules desorbed from the surface of a silicon wafer. MPRI was accomplished by using 280-nm laser radiation and operated at 3×10^5 W/cm^2.

the resonant excitation steps becomes saturated. Extrapolating the functional dependence in Figure 9 at high laser intensity to $x = 0$, an intercept of $\sim 2 \times 10^5$ W/cm^2 is obtained. Interestingly, the x intercept of the linear curve shown in Figure 10 occurs in the 10^5 W/cm^2 range as expected.

Although both carbazole and pyrene are classified as environmental pollutants, one of the most toxic and highly carcinogenic PAC's is benzo[*a*]pyrene ($C_{20}H_{12}$). The detection of this particular molecule, which is present in trace amounts in soil, air, and water samples, is of widespread interest. A TOF mass spectrum of benzo[*a*]pyrene ion desorbed from the surface of a silicon target is shown in Figure 11. For analysis, the laser was tuned to 280 nm at a power density of 3×10^5 W/cm^2. As for pyrene and carbazole, a large molecular ion peak is found without fragmentation. Moreover, by use of a clean silicon wafer as a substrate, the amount of nonresonant impurity ionization is minimized, yielding a very clean TOF mass spectrum with excellent signal-to-noise (S/N) and signal-to-background (S/B) ratios. Interestingly, a small peak occurring at $(M + 13)^+$ is observed. The source of this signal is unknown; however, the formation mechanism may involve (CH) attachment to the molecular ion unit. Alternatively, this moiety may simply correspond to a sample impurity. As the laser intensity is increased to $\sim 2 \times 10^6$ W/cm^2, the benzo[*a*]pyrene molecule extensively photofragments, losing sequential carbon atoms as illustrated in Figure 12. The degree of fragmentation can be adjusted simply by varying the laser intensity. This idea of "tunable" fragmentation has been observed and employed as a means of sequencing peptides

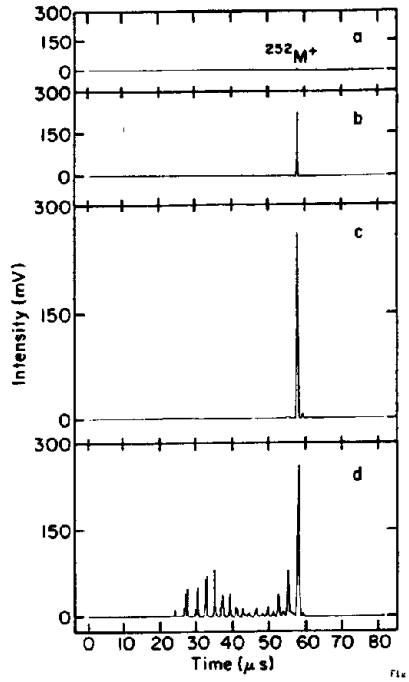

Figure 12. Time-of-flight MPRI mass spectra of benzo[*a*]pyrene ion desorbed from a silicon surface at various 280-nm laser intensities: (a) 1.9×10^4 W/cm^2; (b) 1.2×10^5 W/cm^2; (c) 3.0×10^5 W/cm^2; (d) 2.0×10^6 W/cm^2.

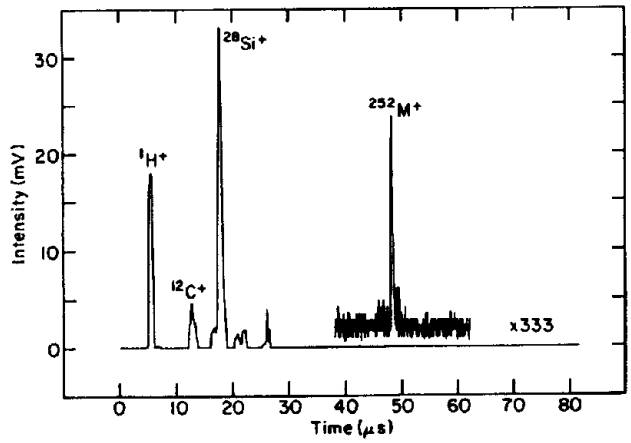

Figure 13. Time-of-flight positive SIMS spectrum of benzo[*a*]pyrene ions desorbed from a silicon surface by using a 815-ns incident Ar^+ ion pulse.

(*24*). The results presented in Figure 12 illustrate the importance of performing fundamental studies in characterizing/optimizing MPRI detection of ion desorbed molecules before any trace analytical experiments are attempted, especially for analysis of complex mixtures of PAC's. The SIMS spectrum of benzo[*a*]pyrene is shown in Figure 13. Along with intense peaks of $^1H^+$, $^{12}C^+$, and $^{28}Si^+$, a weak M^+ ion signal is observed whose intensity is ~1000-fold less than the MPRI signal shown in Figure 11. It is also of interest to note that there is little ion-beam-induced fragmentation associated with benzo[*a*]pyrene desorption. This observation is also consistent with the MPRI results.

Finally, we have attempted to detect the presence of larger molecules whose geometric sizes approach the diameter of biological molecules. These types of molecules have been successfully analyzed by SIMS (*2*) and FAB (*25*) experiments over the last several years. For this study, we chose coronene ($C_{24}H_{12}$) since computer simulations of the desorption event suggest that minimal fragmentation is expected (*26*). A TOF mass spectrum of coronene present on the surface of a silicon substrate is shown in Figure 14. The data indicate an intense

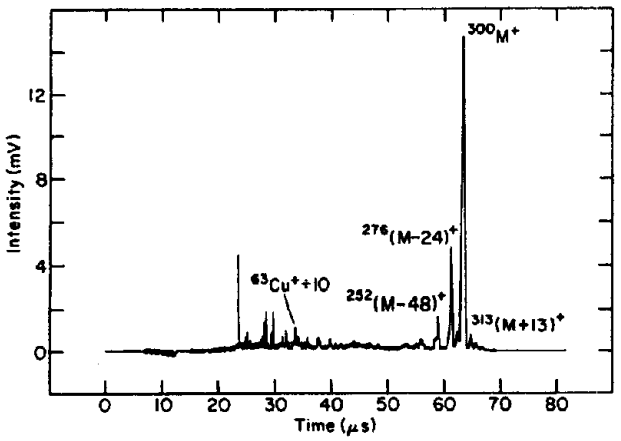

Figure 14. Time-of-flight mass spectrum of a thick film of coronene molecules desorbed from the surface of silicon. MPRI was accomplished by using 280-nm laser radiation and operated at 1.6×10^6 W/cm^2.

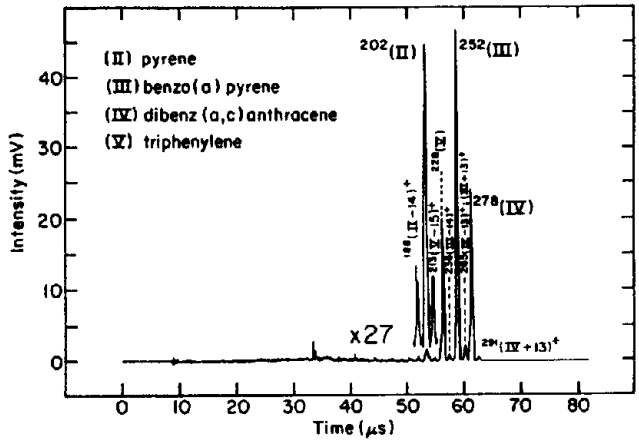

Figure 15. Time-of-flight MPRI mass spectrum of a simulated complex mixture. The spectrum was obtained by use of $\sim 10^{-12}$ mol of each PAC labeled in the insert. MPRI was accomplished by using 280-nm laser radiation and operated at a power density of 1.6×10^6 W/cm^2.

molecular ion peak at 300 amu with minor fragmentation either from the ion beam or the postionization laser, a result supporting the computer simulations. In addition, a peak occurring at $(M + 13)^+$ is observed for coronene that was also seen for benzo[*a*]pyrene desorption. This experiment also implies that a large variety of molecules can be examined with our approach, provided, of course, that their spectroscopic characteristics are commensurate with the laser excitation source.

Control over molecular ion fragmentation opens the possibility for the direct analysis of mixtures of closely related PAC's using MPRI detection. To demonstrate this possibility, a simulated sample was prepared consisting of benzo[*a*]pyrene, dibenz[*ac*]anthracene, triphenylene, and pyrene. A 1:1 benzene solution comprising all four molecules was deposited onto a clean silicon wafer and air dried. The theoretical concentration of each molecule in the analysis zone was $\sim 10^{-12}$ mol assuming uniform deposition. The MPRI TOF mass spectrum of the mixture is shown in Figure 15. The laser was tuned to 280 nm and operated at a modest power density of $\sim 1 \times 10^6$ W/cm^2. There are three intense peaks associated with dibenz[*ac*]anthracene, benzo[*a*]pyrene, and triphenylene and a lower intensity pyrene signal. Note also that the peak intensities for all four molecules are not equal, even though the solution was equimolar with respect to each compound. There are several possible explanations for the observed intensity variations: (i) nonuniform distribution of samples across the target, (ii) different photoabsorption cross sections leading to nonuniform detection efficiencies, and (iii) different sublimation rates due to different vapor pressures of each compound. Nonetheless, these preliminary results suggest that direct mixture analysis will be an important future application of this methodology.

CONCLUSION

The direct MPRI of neutral molecules desorbed from surfaces by ion beams appears to be a significant new approach to surface analysis. In this work, we have shown preliminary mass spectra for a variety of PAC's adsorbed onto gold or silicon substrates. The spectra are of comparable quality to those obtained by laser desorption. Of particular interest is that it is possible to resonantly ionize these molecules with controlled photofragmentation, even though the desorption process itself excites the target molecule to a variety of rotational and vibrational states. This aspect is of critical importance for surface analysis since there are only a limited number of surface molecules. Unfortunately the criterion of efficient sampling precludes the use of supersonic beams to cool these excited molecules into their ground state.

We are most encouraged by the subfemtomole detection limits already reported in these preliminary measurements. It is anticipated that these limits may easily be reduced by another 10–100-fold. For example, by narrowing the incident ion pulse width to the order of 1 μs, the overlap efficiency of the desorbed molecules with the laser beam is increased by a factor of 2. The availability of higher laser powers would also allow us to increase the ionization volume. As yet, we do not have a good feel about the magnitude of the ionization efficiency. If this number is low, there are many approaches to increasing it, using multicolor experiments. It is preferable to employ a low-power ultraviolet (UV) laser pulse for the resonance step, combined with a higher power visible or infrared (IR) pulse for ionization. The use of vacuum UV radiation to produce single-photon ionization also appears to be a promising new approach to produce molecular ions with high yields (*27*). The efficiency of the reflectron analyzer can also be increased by incorporating a gridless design and by increasing postaccelerating potentials to improve MCP performance. This latter point is particularly relevant for detecting high molecular weight molecules. Finally, we have noted some signal loss due to the sublimation of PAC's in the vacuum environment. This problem is being solved by adding a liquid nitrogen cooling attachment to both the sample transfer arm and the sample manipulator.

The combination of ion-beam-induced desorption with MPRI detection offers a number of unique features when compared to competing methods. As already noted, most of the desorbed material is neutral rather than ionic, producing an intrinsic sensitivity advantage over SIMS. Perhaps more importantly, however, is the fact that ion beams can be focused to spot sizes of 200 Å or less and that the sample is desorbed specifically from the top one or two layers of the solid. With the high sensitivity of MPRI detection, it now appears feasible to take advantage of these important characteristics to image desorbed species with molecular specificity *and* high spatial resolution. It will also be of interest to examine the possible use of MPRI to detect high molecular weight samples. This is, of course, already an important application of SIMS. We have obtained preliminary results on polystyrene films, for example, that produce measurable signals to molecular weights up to 1000 by ionization with 280-nm photons (*28*). In summary, then, we believe this initial study on PAC's demonstrates an important new methodology and points toward a number of future novel experimental schemes.

LITERATURE CITED

(1) Grade, H.; Winograd, N.; Cooks, R. G. *J. Am. Chem. Soc.* **1977**, *99*, 7725–7726.

(2) Benninghoven, A. *Surf. Sci.* **1973**, *35*, 427–457.
(3) Land, D. P.; Tai, T.-L.; Lindquist, J. M.; Hemminger, J. C.; McIver, R. T., Jr. *Anal. Chem.* **1987**, *59*, 2924–2927.
(4) Posthumus, M. A.; Kistemaker, P. G.; Meuzelaar, H. L. C.; TenNoever de Brauw, M. C. *Anal. Chem.* **1978**, *50*, 985–991.
(5) Williams, P.; Sundqvist, B. *Phys. Rev. Lett.* **1987**, *58*, 1031–1034.
(6) Kimock, F. M.; Baxter, J. P.; Winograd, N. *Nucl. Instrum. Methods Phys. Res.* **1983**, *218*, 287–292.
(7) Winograd, N.; Baxter, J. P.; Kimock, F. M. *Chem. Phys. Lett.* **1982**, *88*, 581–584.
(8) Harrison, D. E., Jr.; Kelly, P. W.; Garrison, B. J.; Winograd, N. *Surf. Sci.* **1978**, *76*, 311–322.
(9) Winograd, N.; Garrison, B. J. *Methods of Surface Characterization*; Plenum: New York, 1990; Vol. 2, in press.
(10) Pappas, D. L.; Hrubowchak, D. M.; Ervin, M. H.; Winograd, N. *Science* **1989**, *243*, 64–66.
(11) Price, D. *Trends Anal. Chem.* **1990**, *9*, 21–25.
(12) Winograd, N.; Garrison, B. J.; Harrison, D. E., Jr. *J. Chem. Phys.* **1980**, *73*, 3473–3479.
(13) Corderman, R. R.; Engelking, P. C.; Lineberger, W. C. *Appl. Phys. Lett.* **1980**, *36*, 533–535.
(14) Snowdon, K. J.; Heiland, W.; Taglauer, E. *Phys. Rev. Lett.* **1981**, *46*, 284–287.
(15) Lubman, D. M.; Tembreull, R. *Anal. Instrum.* **1987**, *16*, 117–131.
(16) Hahn, J. H.; Zenobi, R.; Zare, R. N. *J. Am. Chem. Soc.* **1987**, *109*, 2842–2843.
(17) Kimock, F. M.; Baxter, J. P.; Pappas, D. L.; Kobrin, P. H.; Winograd, N. *Anal. Chem.* **1984**, *56*, 2782–2791.
(18) *Handbook of Chemistry and Physics*, 63rd ed.; Weast, R. C., Ed.; The Chemical Rubber Company: Cleveland, OH, 1982; p E-72.
(19) Hager, J. W.; Wallace, S. C. *Anal. Chem.* **1988**, *60*, 5–10.
(20) *Handbook of Polycyclic Hydrocarbons, Part A: Benzenoid Hydrocarbons*; Dias, J. R., Ed.; Elsevier Science Publishers: New York, 1987.
(21) Becker, C. H.; Gillen, K. T. *Anal. Chem.* **1984**, *56*, 1671–1674.
(22) Grotemeyer, J.; Lindner, J.; Köster, C.; Schlag, E. W. *J. Mol. Struct.* **1990**, *217*, 51–68.
(23) Winograd, N. *Resonance Ionization Spectroscopy 1988, Proceedings of the Fourth International Symposium on Resonance Ionization Spectroscopy and its Applications*; Conference Series 94; The Institute of Physics: Bristol and Philadelphia, 1988; pp 183–187.
(24) Grotemeyer, J.; Schlag, E. W. *Org. Mass Spectrom.* **1988**, *23*, 388–396.
(25) Barber, M.; Bordoli, R. J.; Sedgwick, R. D.; Tyler, A. N. *Nature* **1981**, *293*, 270–275.
(26) Garrison, B. J. *Int. J. Mass Spectrom. Ion Phys.* **1983**, *53*, 243–254.
(27) Schühle, U.; Pallix, J. B.; Becker, C. H. *J. Am. Chem. Soc.* **1988**, *110*, 2323–2324.
(28) Hrubowchak, D. M.; Ervin, M. H.; Winograd, N. Unpublished results.

RECEIVED for review August 17, 1990. Accepted October 31, 1990. We are grateful to the National Science Foundation, the Office of Naval Research, the Department of Energy, and the IBM Corporation for the financial support of this work.